ACS APPLIED MATERIALS & INTERFACES

Research Article

www.acsami.org

Polyaniline/Carbon Nanotube Sheet Nanocomposites: Fabrication and Characterization

Jae-Woo Kim,*[,†] Emilie J. Siochi,*[,‡] Jennifer Carpena-Núñez,[‡] Kristopher E. Wise,[‡] John W. Connell,[‡] Yi Lin,[†] and Russell A. Wincheski[§]

[†]National Institute of Aerospace, Hampton, Virginia 23681, United States

[‡]Advanced Materials and Processing Branch, and [§]Nondestructive Evaluation Science Branch, NASA Langley Research Center, Hampton, Virginia 23681, United States

Supporting Information

ABSTRACT: Practical approaches are needed to take advantage of the nanometer-scale mechanical properties of carbon nanotubes (CNTs) at the macroscopic scale. This study was conducted to elucidate the salient factors that can maximize the mechanical properties of nanocomposites fabricated from commercially available CNT sheets. The CNT sheets were modified by stretching to improve CNT alignment and in situ polymerization using polyaniline (PANI), a π-conjugated conductive polymer, as a binder. The resulting CNT nanocomposites were subsequently postprocessed by hot pressing and/or high temperature treatment to carbonize the PANI as a means to improve mechanical properties. The PANI/CNT nanocomposites demonstrated significant improvement in mechanical properties compared to pristine CNT sheets. The highest specific tensile strength of PANI/stretched CNT nanocomposite was 484 MPa/(g/cm^3), which was achieved in a sample with ~42 wt % of PANI. This specimen was fabricated by in situ polymerization followed by hot pressing. The highest specific Young's modulus of 17.1 GPa/(g/cm^3) was measured on a sample that was hot-pressed and carbonized. In addition, the highest DC-electrical conductivity of 621 S/cm was obtained on a sample prepared by in situ polymerization of PANI on a stretched CNT sheet.

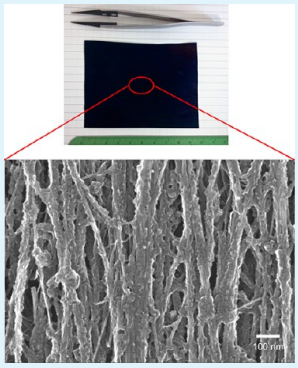

KEYWORDS: *carbon nanotube, polyaniline, structural nanocomposites*

INTRODUCTION

Carbon nanotubes (CNTs) have been shown to possess an outstanding combination of mechanical, electrical, and thermal properties at the nanoscale. The measured values for their elastic moduli range from 1.28 to 1.8 TPa.[1,2] CNTs have exhibited breaking strengths ranging from 11 GPa to 63 GPa[3,4] and failure strain of 1.6%[4] under a tensile load. However, these promising mechanical properties have not been realized in macroscale CNT nanocomposites fabricated by conventional methods,[5−8] because of the weak load transfer between tubes or tube bundles. There is a need for a significant research effort directed toward controlling the interactions between nanotubes, because of the critical role they play in load transfer.

Utilizing the full mechanical capabilities of individual CNTs is critical to attaining structural properties significantly higher than those of state-of-the-art carbon fiber-reinforced polymer (CFRP) composites. Most studies on structural applications of CNTs have focused on attempts to improve dispersion of nanoinclusions in structural polymer matrices. However, this approach has yet to achieve mechanical properties that compete with CFRPs,[9,10] because of poor intertube load transfer, insufficient CNT alignment, and physical defects created during processing and fabrication. In addition, the fabrication of high volume fraction CNT nanocomposites by doping polymer matrices with CNTs is difficult, because of CNT aggregation. Practical use of these nanomaterials will require the development of processes for achieving CNT alignment while also creating stable and strong linkages between CNTs with minimal defects. Several approaches have been developed to introduce cross-linking between CNT shells, including electron beam irradiation,[11−15] application of large compressive forces,[16,17] and chemical treatments.[18−20] These approaches were somewhat successful in improving tube-to-tube load transfer, which improved mechanical properties, but they also introduced unwanted defects in the CNTs and may be difficult to scale up for practical macroscale applications. Alternative approaches including the use of spinnable CNT forests as a starting material, physical densification, and alignment of CNTs by solvent treatments[21] and fabrication using a prepreg-like process[22] have also been developed. The mechanical properties obtained from these materials are quite promising, but scale-up for large nanocomposite structure fabrication still poses significant challenges, especially with regard to the economic feasibility of building up sufficient laminate thickness without introducing defects. In fact, the mechanical properties of these

Received: May 30, 2013
Accepted: August 8, 2013
Published: August 28, 2013

 © 2013 American Chemical Society

nanocomposites were shown to decrease as the nanocomposite thickness increased.[22]

CNT sheets are a promising format for producing high-performance polymer nanocomposites with a high volume fraction of CNTs. Although these sheets are typically available with randomly aligned CNTs, they possess the elasticity to permit stretching to yield significant CNT alignment in the loading direction.[23] These sheets are commercially available in large volumes necessary to determine appropriate processing methods for producing structural nanocomposites. The sheet format also offers advantages such as ease of handling being amenable to physical and chemical modification, and being used as a drop-in substitute for carbon fiber laminates in existing composite processing methods. High-performance polymer/CNT sheet nanocomposites have been reported recently.[24,25] For example, Liang et al. reported multiwalled carbon nanotube (MWCNT) sheet-reinforced bismaleimide (BMI) resin nanocomposites with a tensile strength of ∼2 GPa, a Young's modulus of 169 GPa, and an electrical conductivity of 5500 S/cm along the alignment direction.[25] They demonstrated that a straightforward mechanical stretching method followed by BMI infiltration is capable of producing high-performance nanocomposites with high CNT concentration and low void volume fraction.

Recently, polyaniline has been used as a functionalization or "sizing" agent on CNTs for producing high-volume-fraction CNT fibers,[26] CNT buckypaper,[27] and CNT reinforced epoxy polymer nanocomposites.[28,29] However, most of the previous studies of PANI functionalization of CNTs have focused on attempts to disperse CNTs into solvents or polymer solutions, which were then further processed to make nanocomposites. Mechanical property enhancements were not significant due to low CNT loading content and insufficient CNT alignment in the nanocomposites. In addition to using PANI as a binder, additional heat treatment or carbonization can convert PANI into a nitrogen-containing carbon residue with potential applications in flame-retardant materials and energy conversion and storage.[30−32]

Here, we report systematic approaches to improve mechanical properties of CNT-based structural nanocomposites produced from CNT sheets using a combination of stretching, in situ polymerization, hot pressing, and carbonization. Specifically, in situ polymerization of PANI with highly stretched CNT sheets is a relatively easy process, because of favorable dispersion ($\pi-\pi$) interactions. The PANI essentially locks the physically aligned CNTs in place and does not require a complicated dispersion of CNTs into a solvent or polymer matrix. The demonstrated methods are relatively simple and scalable for structural applications. In addition, the PANI/CNT nanocomposites exhibited good electrical conductivity, making them attractive for multifunctional structural applications.

EXPERIMENTAL SECTION

Materials. The CNT starting materials used in this work were in the form of CNT powder (Bayer multiwalled carbon nanotubes (MWCNTs), Baytubes C150 HP, 99% purity), as well as both untreated (catalyst content: 10.9 wt %, average areal density: 11.0 g/m^2) and acetone-treated (catalyst content: 10.3 wt %, average areal density: 15.5 g/m^2) CNT sheets (Nanocomp Technologies, Inc.). Aniline (Aldrich, 99.8%), ammonium persulfate ($(NH_4)_2S_2O_8$, Aldrich, 98+%), ammonium hydroxide (Fisher, 29.9%) and various organic solvents were used as received.

Nanocomposites. Some of the CNT sheets used in this work were stretched prior to the in situ polymerization step. The sheets were stretched in tension up to 33% strain at a crosshead speed of 1 mm/min at ambient temperature. Stretching was done with either dry sheets or sheets wetted with a solvents such as acetone, ethanol, or *N*-methylpyrrolidone (NMP). Nanocomposites were formed by subjecting the CNT sheet to in situ polymerization in an aniline solution using procedures documented in the literature,[33−37] followed by post-processing with a combination of hot pressing and carbonization. In this study, the CNT powder and sheet were first immersed in an acidic aqueous solution containing various concentrations of aniline. For the powder preparation, the mixed solution of MWCNT and aniline was dispersed in an aqueous 3-(*N*-morpholino)-propanesulfonic acid (MOPS) buffered solution without any additional surfactants or additives.[38] Aniline polymerized on the CNTs surfaces to yield PANI/CNT nanocomposites. Adjusting the aniline monomer concentration in the solution controlled the thickness of the PANI/CNT nanocomposites. PANI/CNT sheet nanocomposites were prepared by in situ polymerization of aniline in an acidic solution bath (1 M HCl) with ammonium persulfate as the oxidant in the presence of CNT sheet. The weight ratio between the CNT sheet and aniline was 1:5, and the molar ratio between the aniline monomer and the oxidant is 1:1. The emeraldine base form (EB, electrically nonconductive) of PANI/CNT sheet nanocomposite was obtained by stirring the as-prepared (emeraldine salt form (ES) - electrically conductive) nanocomposite into a diluted ammonium hydroxide solution (3 wt %) for 15 h. After polymerization, the PANI/CNT nanocomposite was post-processed by hot pressing (Carver, Inc., hydraulic unit, Model No. 3925) at 100 °C and a pressure of ∼1−2 GPa. In addition, some samples were carbonized at up to 2000 °C in an inert atmosphere (N_2) to convert the PANI coating into amorphous carbon (a-C). The carbonization process was conducted in a vacuum furnace (R.D. Webb, Red Devil) at atmospheric pressure and a constant N_2 gas with a flow rate of 2 ft^3/h. Temperature was ramped up at 10 °C/min and then held for 10 min to complete the carbonization. Tension was not applied to the PANI/CNT nanocomposite during the carbonization process.

Characterization. Raman spectroscopy was performed using a Kaiser RAMANRXN1 Microprobe. All measurements were performed at an excitation wavelength of 785 nm and laser output power of 50 mW. Polarization optics were incorporated to enable acquisition of Raman spectra as a function of angle between the natural rolling direction of the sheets and the polarization direction. Thermogravimetric analysis (TGA) (Netzsch, Model TG 209 F1) and differential scanning calorimetry (DSC) (Netzsch, Model DSC 204 F1) were carried out under nitrogen at heating rates of 5 °C/min and 10 °C/min, respectively.

The pristine CNT sheets and PANI/CNT nanocomposites were mechanically tested (at least five samples) at room temperature using an Instron Model 5848 Microtester. The measured force-displacement data were used to calculate specific elastic modulus (Young's modulus), specific ultimate strength, and ultimate tensile strain. The tensile stress was obtained by dividing the measured force by the cross-sectional area of the PANI/CNT sheet nanocomposites, which was determined with a micrometer and confirmed by microscopy measurements. All data were normalized by the density of the PANI/CNT sheet nanocomposites, as determined by the sample dimension and weight. The tensile testing method was based on ASTM standards, including ASTM D882 ("Standard Test Method for Tensile Properties of Thin Plastic Sheeting") and ASTM D1708 ("Standard Test Method for Tensile Properties of Plastics by Use of Microtensile Specimens"). The tensile samples were cut into rectangular strips 5.08 ± 0.03 mm wide, using a JDC precision sample cutter (Thwing-Albert Instrument Company). The thickness of the prepared nanocomposites ranged from 20 μm to 50 μm. PANI content in the prepared PANI/CNT nanocomposites ranged from 42 wt % to 58 wt %, except for the carbonized nanocomposites. The measured densities of pristine CNT sheet, in situ polymerized PANI/CNT, hot-pressed PANI/CNT and carbonized PANI/CNT composites were 0.566 ± 0.011, 0.816 ± 0.147, 1.218 ± 0.143, and 0.636 ± 0.132 g/cm^3, respectively. Gauge length and crosshead speed for the tensile test were set at 10 mm and 10 mm/min, respectively. Strain

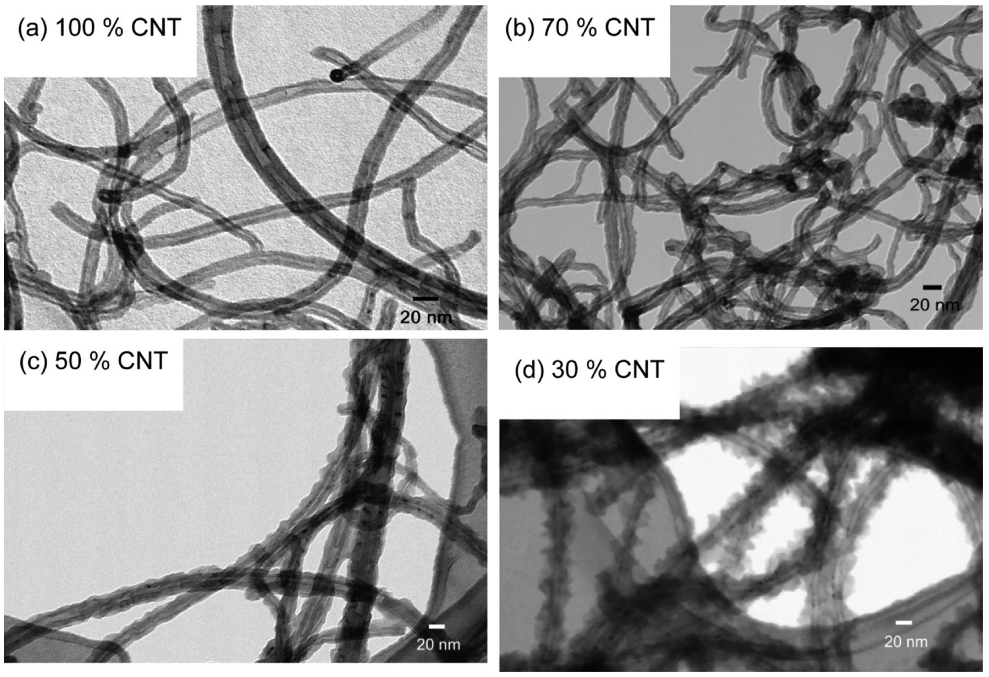

Figure 1. Representative STEM images of (a) 100 wt % CNTs, (b) 70 wt % CNT/30 wt % PANI, (c) 50 wt % CNT/50 wt % PANI, and (d) 30 wt % CNT/70 wt % PANI.

was calculated from crosshead displacement. The Young's modulus was obtained from linear regression at the maximum slope of the corresponding stress−strain curve. Toughness was calculated by measuring the area under stress−strain curve up to failure.

A field emission-scanning electron microscope (FE-SEM, Hitachi Model S-5200) equipped with a scanning transmission electron microscope (STEM) detector was used to image both as-processed PANI/CNT nanocomposites and cross-sectioned samples of failed specimens after a tensile test. A Gatan Microtester 200 stage and Deben controller equipped with a digital optical microscope (Mighty Scope) were used for in situ fracture imaging. DC conductivities of the PANI/CNT nanocomposites were measured with a 4-probe system (Signatone, QuadPro Resistivity Wafer Mapping System).

RESULTS AND DISCUSSION

In Situ Polymerization of Aniline with Individual CNTs. Before applying PANI coating directly to the CNT sheet materials, eight polyaniline nanocomposites with 0, 0.5, 1, 5, 10, 30, 50, and 70 wt % MWCNT were synthesized to understand the interaction between aniline and CNT during in situ polymerization of aniline in buffer-stabilized MWCNT dispersion solutions. The mechanism of in situ polymerization has been discussed previously.[33−37] Dispersion interactions between the π electrons in the aromatic aniline monomers and the extended, delocalized π electron system on the CNTs promoted physical adsorption of the monomers onto the nanotube surface and resulted in a good dispersion of the nanotubes in the aqueous buffer solution. The same dispersion interaction between the CNT and the aniline monomer that yields a good dispersion may also promote polymerization along the CNT to afford PANI-coated MWCNTs. The conversion yield of PANI increased as a function of MWCNT concentration from 64.2% at 0 wt % to 93.2% at 70 wt %. This enhanced conversion suggests that the CNT surface provides reactive sites where polymerization can occur. Increased reactivity can lead to improved reaction efficiency and thus lower production costs if this process were scaled up.

Figure 1 shows STEM images of pristine MWCNTs (Figure 1a), as well as 70 wt % (Figure 1b), 50 wt % (Figure 1c), and 30 wt % (Figure 1d) MWCNT-PANI nanocomposites, respectively. The pristine MWCNT diameters were in the range of 10−25 nm (see Figure 1a). The functionalized MWCNTs were very uniformly and completely coated by a PANI layer (see Figures 1b−d). SEM images revealed a beaded surface on the CNTs, with coating features being increasingly rougher as the PANI concentration increased (see Figures 1c and 1d). The thickness of the PANI layer on the MWCNT surface decreased as the PANI content in the nanocomposites decreased. After in situ polymerization of PANI, the diameters of 30 wt % MWCNT/PANI nanocomposite increased to ∼20−50 nm while the diameters of the 50 wt % MWCNT/PANI hybrid were 10−40 nm. The PANI layer thickness typically ranged from 3 nm to 20 nm. Note that the sidewalls of the MWCNT are not visible under a microscope below 30 wt.% MWCNT concentration due to the presence of a thick layer of PANI.

Fabrication of PANI/CNT Sheet Nanocomposites and Their Mechanical and Electrical Properties. Following the guidance from the above model reactions performed using MWCNTs, PANI/CNT sheet nanocomposites were fabricated by in situ polymerization of aniline monomer onto a pristine CNT sheet (Figure 2a). Figure 2b shows that polymeric materials were well-coated on the CNTs and interconnected between the CNT bundles. After subsequent hot pressing (Figure 2c) or carbonization processes (Figure 2d), the overall CNT network in the nanocomposite was retained, but the morphology of the polymeric coatings exhibited discernible changes. The primary effect of hot-pressing PANI/CNT nanocomposites was increased density of the material, which was due to the reduction of voids within the nanocomposite. In fact, hot pressing reduced the thickness of the PANI/CNT nanocomposites by 10%−50%, depending on the level of stretch and applied pressure. Hot pressing consolidated layers of PANI/CNT sheets to produce macroscale PANI/CNT

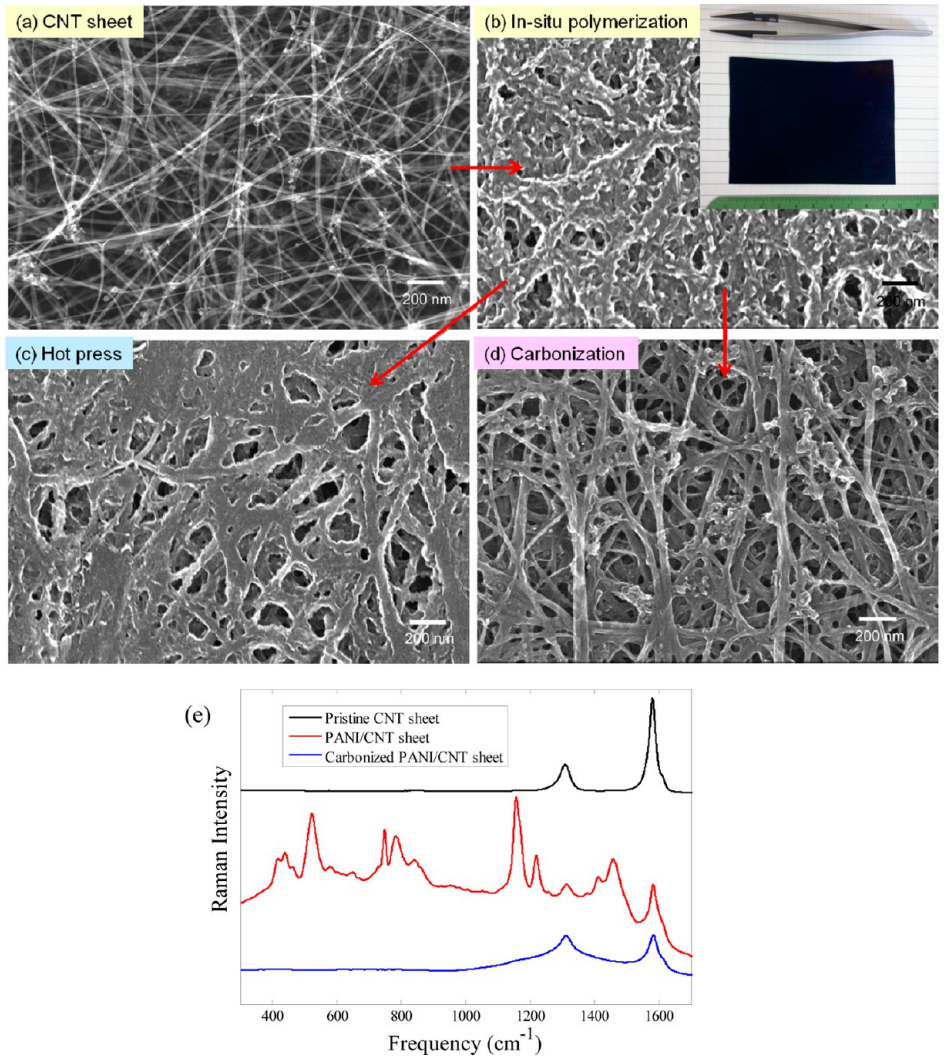

Figure 2. SEM images of (a) the pristine CNT sheet and the PANI/CNT sheet nanocomposites after (b) in situ PANI polymerization and then (c) hot pressing and (d) carbonization. Inset in panel (b) shows a photograph of the as-prepared PANI/CNT nanocomposite. (e) Stacked Raman spectra of pristine CNT sheet, PANI/CNT sheet, and carbonized PANI/CNT sheet. Intensity values for carbonized sample multiplied by a factor of 2. All data acquired with light polarized in the aligned CNT direction of the sheet.

nanocomposites in a process similar to current carbon fiber composite fabrication methods.

Raman spectra of the pristine CNT sheet, PANI/CNT sheet, and carbonized CNT sheet are shown in Figure 2e. The Raman spectroscopy confirmed the uptake of PANI in the PANI/CNT nanocomposite, exhibiting typical bands attributed to the doped PANI.[33,39] Raman results from the carbonized PANI (emeraldine salt (ES) form) were also in good agreement with the literature.[30,40] Specifically, the characteristic Raman bands of the PANI disappeared after heating to 800 °C and two main bands (G- and D-bands) of carbonized nanocomposite were observed. The G- and D-bands were broadened due to increasing disorder and amorphous carbon content, indicating the presence of carbonized PANI in the nanocomposite. Overall weight loss of the PANI/CNT nanocomposites after carbonization at 800 °C in N_2 atmosphere was 30% as determined by TGA (see Figure S1 in the Supporting Information). The thermogram of polyaniline (emerladine base (EB) form) showed a weight loss of 10% from room temperature to 400 °C and a weight loss of 42% from 400 °C to 1000 °C, in good agreement with data reported in the literature.[35,40]

The maximum stretching level achieved with the CNT sheet was 33% strain at a crosshead speed of 1 mm/min. The CNTs were well-aligned along the stretch direction and well-coated by PANI during in situ polymerization, as shown in Figures 3a and 3b. Polarized Raman spectroscopy on a pristine CNT sheet (Figure 3c) and a PANI/CNT nanocomposite (Figure 3d), both stretched and unstretched are also shown. The increased alignment of the CNTs in the stretched sheets is reflected in the increased intensity of the G peak in the Raman polarization spectra aligned with the stretch direction, relative to the G peak for the polarization spectra perpendicular to this axis. This is consistent with results reported in the literature for aligned CNTs.[41]

Figure 4 shows the changes in mechanical properties as a function of the level of stretching for a pristine CNT sheet and various PANI/CNT sheet nanocomposites. The measured specific tensile strength and specific Young's modulus of the untreated CNT sheet were 160 ± 16 MPa/(g/cm^3) and 0.8 ± 0.3 GPa/(g/cm^3), respectively, and the elongation at failure was

dx.doi.org/10.1021/am402077d | ACS Appl. Mater. Interfaces 2013, 5, 8597−8606

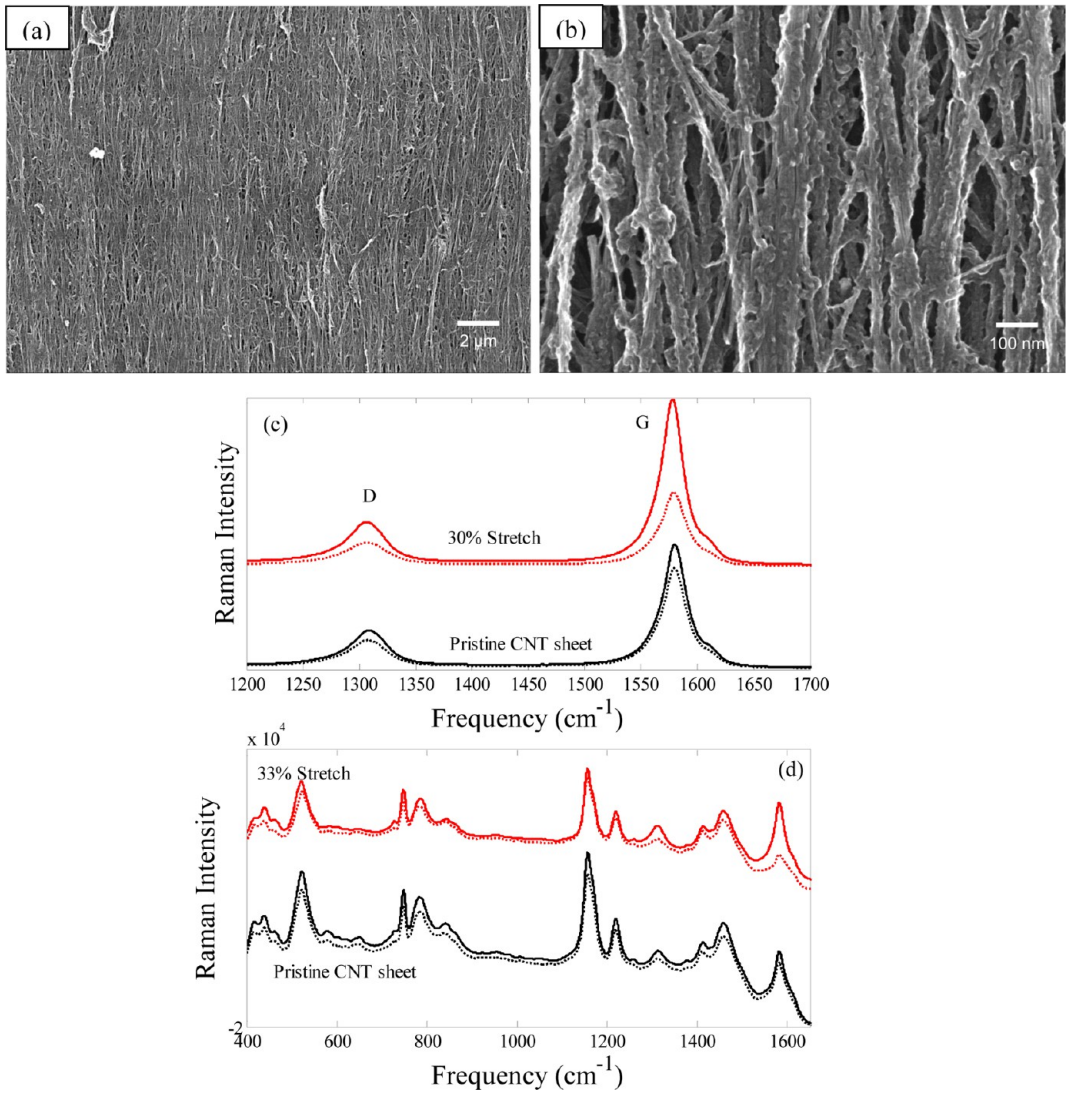

Figure 3. SEM images of 33% stretched CNT sheet modified with PANI; (a) low magnification and (b) high magnification image. Stacked Raman spectra of (c) pristine CNT sheet without and with 30% stretch and (d) PANI/CNT nanocomposites without and with 33% stretch. Solid lines show data acquired with light polarized in the sheet stretching direction and dashed lines show data acquired with polarization optics perpendicular to stretched direction.

50.3 ± 4.5%. In situ polymerization, which resulted in PANI reinforcement of the CNT networks, increased the specific strength to 239 ± 16 MPa/(g/cm^3). The Young's modulus increased by an order of magnitude to 9.0 ± 0.2 GPa/(g/cm^3) compared to the untreated CNT sheet. The specific tensile strength and specific Young's modulus are expected to increase with the stretch level of the PANI/stretched CNT sheet nanocomposites, because of the alignment of the CNTs along the tensile load direction. Stretching the as-manufactured sheets not only increased the alignment of the CNTs in the stretch direction, but also densified the sheet, eliminating some intertubular voids to increase tube packing. Stretching the pristine sheets significantly improves their specific modulus (Figure 4b) and also has a positive, although weaker, effect on their specific strength (Figure 4a). These trends are reversed for the PANI/CNT sheet nanocomposites, for which the specific strength increases sharply with stretching while the specific modulus increases only slightly, although there is significant scatter in the data at higher stretching ratios.

The failure mode in the relatively thick pristine CNT sheet is likely shear sliding between the tubes and layers of CNT sheets. CNT sheet strength is limited by characteristics such as CNT length, type, and quality. In the nanocomposites, the polymer binds the tubes so that intertube slippage is minimized. Clearly, the composition of the polymer is important, because good interfacial interaction between the polymer binder and the CNTs is required for effective load transfer. The CNT alignment has the largest effect on the Young's modulus of the pristine CNT sheets, while their strength is not significantly enhanced due to the weak interfacial shear strength of bare CNTs.[13] The elongation at failure in the pristine CNT sheet, shown in Figure 4c, decreased linearly as a function of the level of stretching while the PANI/CNT nanocomposites showed a plateau at ~10% of elongation in the highly stretched samples. These results suggest that the PANI/CNT nanocomposites from highly stretched (over 20%) CNT sheets are tougher than the pristine CNT sheets with the same level of stretching (Figure 4d), as expected, based on the enhanced strength exhibited by the nanocomposite relative to the pristine CNT

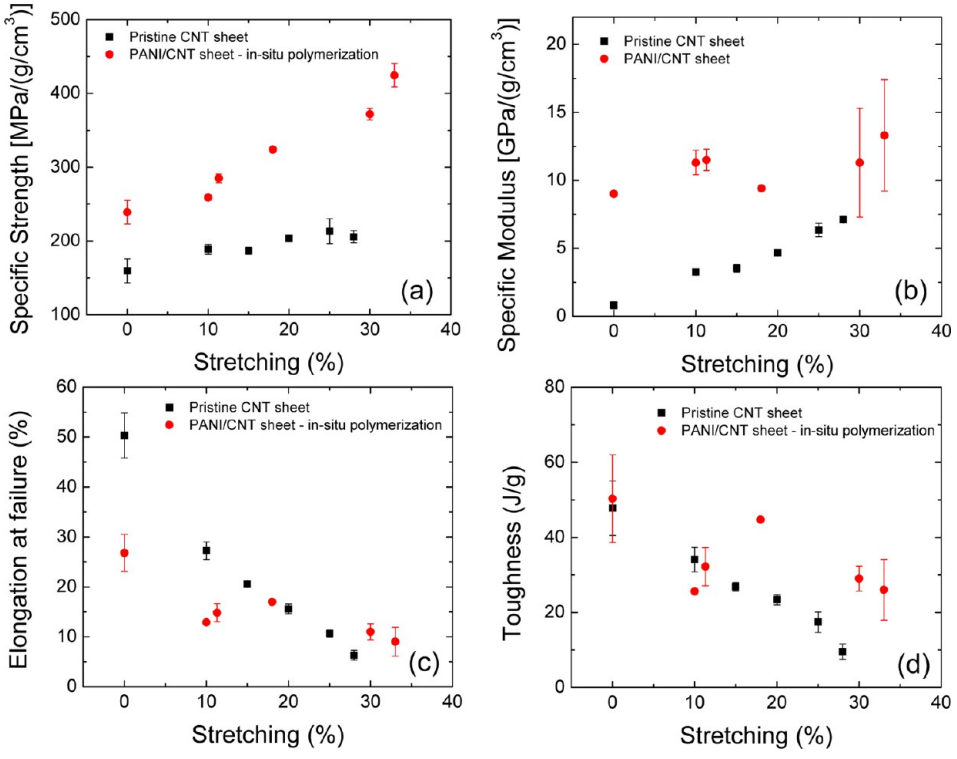

Figure 4. Comparison of the average (a) specific strength, (b) specific modulus, (c) elongation at failure, and (d) toughness of pristine CNT sheet and in situ polymerized PANI treated CNT sheet nanocomposites in terms of the level of stretching. The error bars represent the standard deviation in the values.

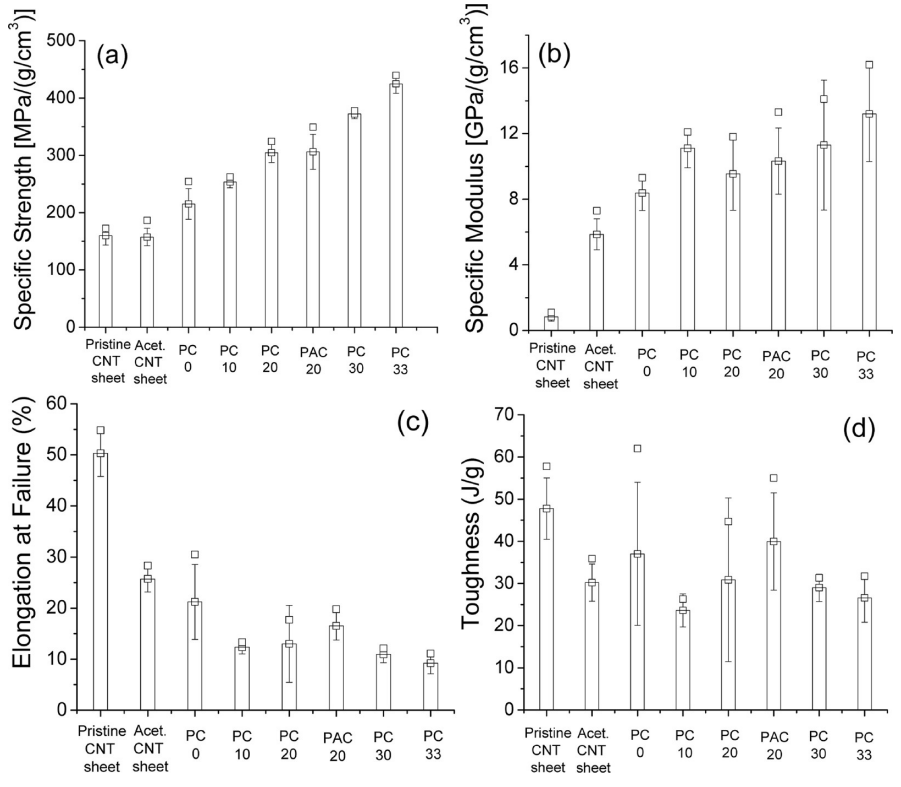

Figure 5. Comparison of the average (a) specific strength, (b) specific modulus, (c) elongation at failure, and (d) toughness of pristine CNT sheet and in situ polymerized PANI treated CNT sheet nanocomposites with unstretched and stretched CNT sheets. The error bars represent the standard deviation in the values. The open squares are the measured maximum values for each sample. The level of stretch of CNT sheet before PANI polymerization was varied as 0, 10, 20, 30, and 33% and the resulting nanocomposites were named as PC0, PC10, PC20, PC30, and PC33, respectively. The PAC20 represents a PANI/stretched CNT sheet nanocomposite prepared with a 20% stretched acetone-treated CNT sheet.

dx.doi.org/10.1021/am402077d | ACS Appl. Mater. Interfaces 2013, 5, 8597−8606

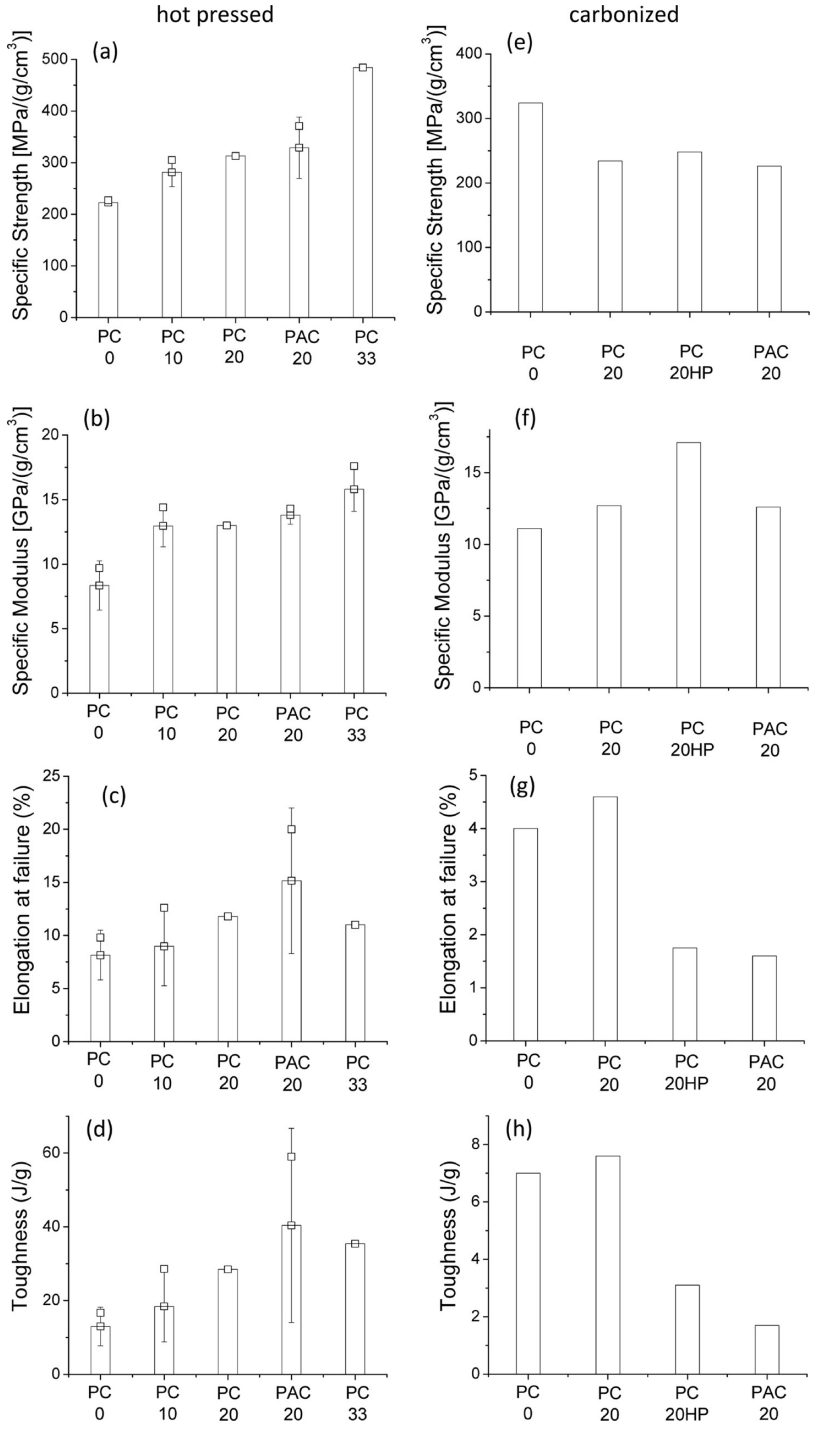

Figure 6. Comparison of the average (a,e) specific strength, (b,f) specific modulus, (c,g) elongation at failure, and (d,h) toughness of PANI/CNT sheet nanocomposites post-processed by hot pressing and carbonization, respectively. The error bars represent the standard deviation in the values. The open squares are the measured maximum values at each sample. The level of stretch of CNT sheet before PANI polymerization was varied as 0%, 10%, 20%, and 33% and the resulting nanocomposites were labeled PC0, PC10, PC20, and PC33, respectively. The PAC20 represents a PANI/stretched CNT sheet nanocomposite prepared with a 20% stretched acetone-treated CNT sheet. The PC20HP represents a PANI/stretched CNT sheet nanocomposite prepared with a 20% stretched CNT sheet and then experienced a hot press before carbonization.

sheet. This indicates that the intertube load transfer and interfacial adhesion between PANI and CNT are much improved by PANI polymerization in relatively dense CNT sheets.

The effects of post-processing treatments on the mechanical properties of the PANI/CNT sheet nanocomposites are summarized in Figures 5 and 6. Methods investigated include solvent treatment, stretching, in situ polymerization (Figure 5), hot pressing, and carbonization (Figure 6). Solvent treatment, especially with acetone, increases CNT sheet density. This densification has little effect on the specific strength, as shown in Figure 5a, but the specific modulus (Figure 5b) increases substantially. Starting with an acetone-treated nancomposite offers no benefit in strength or modulus after stretching, as can

be seen by comparing the properties of the 20% stretched pristine (PC20) and acetone-treated (PAC20) samples in Figures 5a and 5b.

The highest specific tensile strength [484 MPa/(g/cm^3)] was obtained with the PANI/stretched CNT sheet nanocomposites in which the 33% stretched CNT sheet was impregnated with PANI via in situ polymerization, and then consolidated by hot pressing (Figure 6a). Hot pressing also had a small but positive effect on the specific modulus of the nanocomposites (Figure 6b). Despite good adhesion between PANI and the CNTs, the Young's modulus of the hot-pressed PANI/CNT sheet nanocomposites is about an order of magnitude lower than that of the state-of-the-art epoxy/CNT sheet nanocomposites,[25] possibly due to the high void content (Figure 2) in the fabricated nanocomposites. Further infiltration of epoxy resin with as-prepared PANI/CNT sheet nanocomposites could potentially improve the mechanical property by filling in the voids with a structural engineering polymer.

The highest specific Young's modulus, 17.1 GPa/(g/cm^3), was obtained with PANI/stretched CNT sheet nanocomposite after hot pressing and carbonization. Hot pressing reduced voids and densified the nanocomposite to enhance the extent of intertube contacts, thus improving mechanical properties. However, the Young's modulus of this carbonized PANI/CNT nanocomposite is much lower than that of typical engineering carbon fiber-reinforced composites. The anticipated improvement in modulus was not realized, very likely due to the high catalyst content in the starting CNT material. High-temperature carbonization of the PANI/CNT nanocomposites where the CNT contained ~10 wt % iron catalyst provides a degradation mechanism from oxidation of the CNT by oxygen released from the iron oxide catalyst. This reaction results in the generation of voids that severely weaken the mechanical property of the carbonized PANI/CNT nanocomposites.

Generally, hot pressing had a larger effect on tensile strength, while carbonization had a greater impact on the Young's modulus. Elongation at failure decreased considerably after in situ polymerization, and even more significantly upon stretching and carbonization. As a result, toughness also decreased significantly, especially after the carbonization process. As shown in Figure 6h, the toughnesses of the PANI/stretched CNT sheet nanocomposites were in the range of 1.7−7.6 J/g after carbonization, while that of the untreated CNT sheet was 47.8 ± 7.3 J/g (Figure 5d). While hot pressing improved the strength of the PANI/CNT nanocomposites, there was minimal decrease in toughness to 40 J/g at 20% stretch, as shown in Figure 6d. The toughness value is somewhat lower than that of state-of-the-art CNT yarns (close to 100 J/g).[20,42] In general, the form of PANI, i.e. emeraldine salt (ES, electrically conductive form) or emeraldine base (EB, nonconductive form) did not affect the mechanical properties of the resultant nanocomposite. The reported mechanical data were measured with the ES form of PANI.

The DC-electrical conductivity of the PANI/CNT nanocomposites along the CNT aligned direction was measured using a four-point probe, and the results are summarized in Figure 7. The DC-electrical conductivity of the pristine CNT sheet was 342 ± 37 S/cm. The DC-electrical conductivity had a significant dependence on the initial form of PANI used; the highest values were obtained with the PANI/stretched CNT sheet nanocomposites (621 ± 10 S/cm) in which the PANI was in the emeraldine salt form. Generally, hot pressing increased the electrical conductivity in both PANI forms,

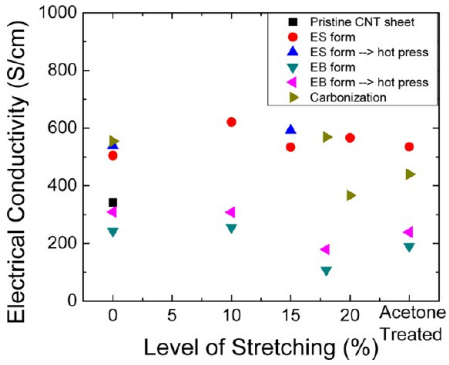

Figure 7. DC-electrical conductivity of the processed PANI/CNT sheet nanocomposites. The abbreviations "ES" and "EB" stand for emeraldine salt (electrically conductive form) and emeraldine base (electrically nonconductive form), respectively.

because of densification of the materials. The electrical conductivity of carbonized PANI/CNT nanocomposite was not influenced by the form of PANI.

Failure Mechanism of Pristine CNT Sheet and PANI/CNT Nanocomposites. The failure mechanisms of the pristine CNT sheets and the PANI/CNT nanocomposites were examined at the micrometer scale with an in situ tensile tester (Gatan Microtest 200 stage and Deben controller) equipped with an optical and an electron microscope. A strip of the pristine CNT sheet was placed under a tensile strain and its failure behavior was observed with an optical microscope (see Supporting Information, video clip 1). Interpretation of the failure mechanism of the pristine CNT sheets is complicated by the variations in CNT sheet morphologies.[43] Failure mechanisms noted within the pristine CNT sheet included breaking, sliding, debundling, telescoping, and delamination. The pristine CNT sheet is composed of many layers of highly entangled, mostly double-walled CNTs held together by both van der Waals interactions between the tubes and the bundles and physical entanglements. Pristine CNT sheets tended to fail via a combination of mechanisms that include surface fracture and sliding of the bundles during stretching, as well as delamination of the separated layers, mostly close to the grips due to the auxetic behavior under a tensile load.[44] However, the failure mechanism changed with the addition of PANI binder (see Supporting Information, video clip 2). PANI served to bind the CNT networks preventing delamination of the CNT layers. Failure was initiated at one of the sample edges by localized stress during necking under a tensile load, and then propagated unidirectionally with simultaneous failure cracks, as shown in Figure 8 and video clip 2 in the Supporting Information. Multiple cracks developed from uneven load distribution in the materials and were observed in both the PANI/CNT and the hot-pressed PANI/CNT nanocomposites, as shown in Figures 8b and 8c, respectively. The PANI-coated CNTs oriented in the direction of the tensile load were partially broken first and subsequently telescoped from the CNT bundles or individual tubes during the continuous stretching. Telescoped CNTs bridged the cracks (marked by arrows in Figures 8b and 8c) and transferred load until complete failure of the material occurred. Telescoped CNTs were cleaner and thinner (Figure 8d), compared to the tube bundles in the PANI/CNT nanocomposites. Considering the mechanical data of the stretched samples (Figures 4 and 5), these studies strongly suggest that better alignment of the CNTs in the axial direction

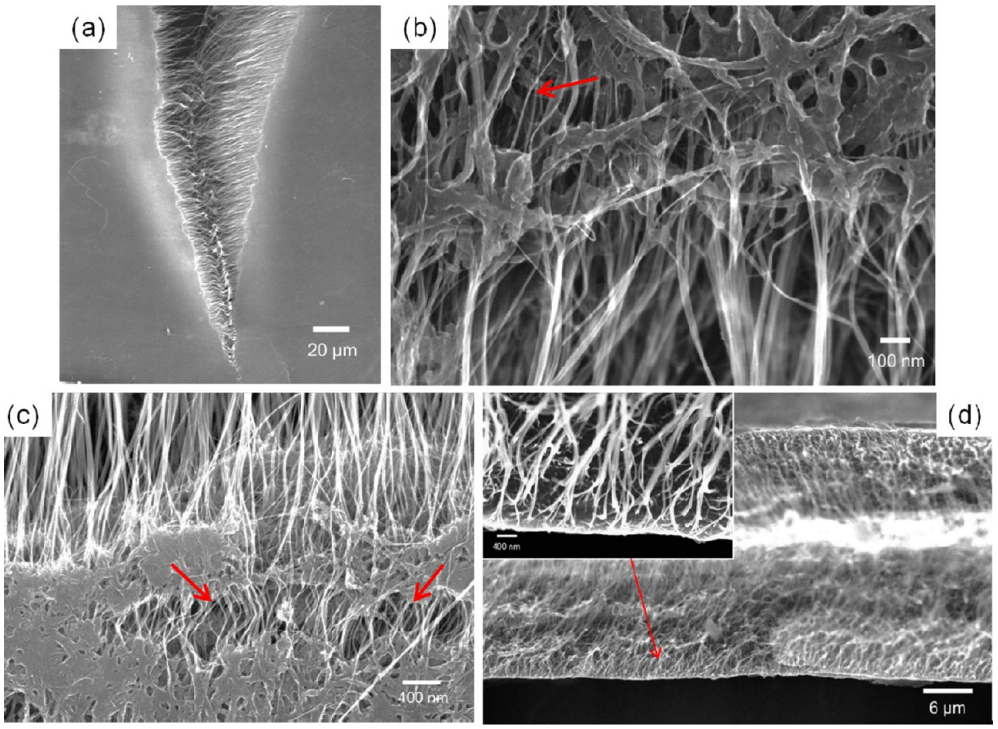

Figure 8. SEM images of the PANI/CNT nanocomposites: (a) half-failed during in situ tensile testing and (b) at the failed site after tensile testing. SEM images of the hot-pressed PANI/CNT nanocomposites (c) in the failed site and (d) in a cross-sectional view after tensile testing.

and better adhesion between the tube and the polymer binder to reduce in-plane failure are critical factors to achieving maximum load transfer in the CNT-based nanocomposites.

CONCLUSION

Various approaches to enhancing mechanical properties of carbon nanotube (CNT) sheets for structural applications, including a combination of solvent treatment, stretching, in situ polymerization, hot pressing, and carbonization, were investigated. The CNTs and CNT bundles were packed more closely when stretched, with PANI effectively locking the aligned CNTs and their bundles in place to improve load transfer and prevent shear sliding between the tubes as well as between the CNT layers within the sheet macrostructure. Even though hot pressing and carbonization of the PANI/CNT nanocomposites improved the specific strength and modulus of the materials, respectively, it can be concluded that improving the overall mechanical properties of CNT sheet toward "super strong" nanocomposites will require both improved CNT alignment and optimized binding at the interface between adjacent CNT bundles.

ASSOCIATED CONTENT

Supporting Information

TGA and DSC thermograms of pristine CNT sheet, PANI powder (EB), PANI(EB)/Bayer MWCNT, and PANI(EB)/CNT sheet. This material is available free of charge via the Internet at http://pubs.acs.org.

AUTHOR INFORMATION

Corresponding Author

*Tel.: 1-757-864-1383 (J.-W.K.), 1-757-864-4279 (E.J.S.). Fax: 1-757-864-8312 (J.-W.K., E.J.S.). E-mail: jae-woo.kim-1@nasa.gov (J.-W.K.), Emilie.j.siochi@nasa.gov (E.J.S.).

Notes

The authors declare no competing financial interest.

ACKNOWLEDGMENTS

The authors thank Nanocomp Technologies, Inc., for supplying the pristine CNT materials. J.C.N. acknowledges support by the Space Technology Research Fellowship (Grant No. NNX11AN21H), provided by the NASA Office of the Chief Technologist.

REFERENCES

(1) Wong, E. W.; Sheenhan, P. E.; Lieber, C. M. *Science* **1997**, *277*, 1971−1975.
(2) Treacy, M. M. J.; Ebbesen, T. W.; Gibson, J. M. *Nature* **1996**, *381*, 678−680.
(3) Yu, M.-F.; Lourie, O.; Dyer, M. J.; Moloni, K.; Kelly, T. F.; Ruoff, R. S. *Science* **2000**, *287*, 637−640.
(4) Zhu, Y.; Espinosa, H. D. *Proc. Natl. Acad. Sci. U.S.A.* **2005**, *102*, 14503−14508.
(5) Xie, X. L.; Mai, Y. W.; Zhou, X. P. *Mater. Sci. Eng., R.* **2005**, *49*, 89−112.
(6) Moniruzzaman, M.; Winey, K. I. *Macromolecules* **2006**, *39*, 5194−5205.
(7) Coleman, J. N.; Khan, U.; Blau, W. J.; Gun'ko, Y. K. *Carbon* **2006**, *44*, 1624−1652.
(8) Spitalsky, Z.; Tasis, D.; Papagelis, K.; Galiotis, C. *Prog. Polym. Sci.* **2010**, *35*, 357−401.
(9) Dalton, A. B.; Collins, S.; Muñoz, E.; Razal, J. M.; Ebron, V. H.; Ferrari, J. P.; Coleman, J. N.; Kim, B. G.; Baughman, R. H. *Nature* **2003**, *423*, 703.
(10) Liu, K.; Sun, Y.; Lin, X.; Zhou, R.; Wang, J.; Fan, S.; Jiang, K. *ACS Nano* **2010**, *4*, 5827−5834.
(11) Kis, A.; Csanyi, G.; Salvetat, J.-P.; Lee, T.-N.; Couteau, E.; Kulik, A. J.; Beniot, W.; Brugger, J.; Forro, L. *Nat. Mater.* **2004**, *3*, 153−157.
(12) Krasheninnikov, A. V.; Banhart, F. *Nat. Mater.* **2007**, *6*, 723−733.

(13) Peng, B.; Locascio, M.; Zapol, P.; Li, S.; Mielke, S.; Schatz, G. C.; Espinosa, H. D. *Nat. Nanotechnol.* **2008**, *3*, 626−631.
(14) Filleter, T.; Bernal, R.; Li, S.; Espinosa, H. D. *Adv. Mater.* **2011**, *23*, 2855−2860.
(15) Filleter, T.; Espinosa, H. D. *Carbon* **2013**, *56*, 1−11.
(16) Braga, S. F.; Galvão, D. S. *Chem. Phys. Lett.* **2006**, *419*, 394−399.
(17) Zhang, Z.; Li, Q. *ACS Nano* **2010**, *4*, 312−316.
(18) Shim, B. S.; Zhu, J.; Jan, E.; Critchley, K.; Ho, S.; Podsiadlo, P.; Sun, K.; Kotov, N. A. *ACS Nano* **2009**, *3*, 1711−1722.
(19) Yi, B.; Rajagopalan, R.; Foley, H. C.; Kim, U. J.; Liu, X.; Eklund, P. C. *J. Am. Chem. Soc.* **2006**, *128*, 11307−11313.
(20) Boncel, S.; Sundaram, R. M.; Windle, A. H.; Koziol, K. K. K. *ACS Nano* **2011**, *5*, 9339−9344.
(21) Li, S.; Zhang, X.; Zhao, J.; Meng, F.; Xu, G.; Yong, Z.; Jia, J.; Zhang, Z.; Li, Q. *Compos. Sci. Technol.* **2012**, *72*, 1402−1407.
(22) Di, J.; Hu, D.; Chen, H.; Yong, Z.; Chen, M.; Feng, Z.; Zhu, Y.; Li, Q. *ACS Nano* **2012**, *6*, 5457−5464.
(23) Sreekumar, T. V.; Liu, T.; Kumar, S.; Ericson, L. M.; Hauge, R. H.; Smalley, R. E. *Chem. Mater.* **2003**, *15*, 175−178.
(24) Wang, Z.; Laing, Z.; Wang, B.; Zhang, C.; Kramer, L. *Composites, Part A* **2004**, *35*, 1225−1232.
(25) Cheng, Q.; Bao, J.; Park, J. G.; Laing, Z.; Zhang, C.; Wang, B. *Adv. Funct. Mater.* **2009**, *19*, 3219−3225.
(26) Chen, T.; Cai, Z.; Qiu, L.; Li, H.; Ren, J.; Lin, H.; Yang, Z.; Sun, X.; Peng, H. *J. Mater. Chem. A* **2013**, *1*, 2211−2216.
(27) Blighe, F. M.; Diamond, D.; Coleman, J. N.; Lahiff, E. *Carbon* **2012**, *50*, 1447−1454.
(28) Xu, J.; Yao, P.; Jiang, Z.; Liu, H.; Li, X.; Liu, L.; Li, M.; Zheng, Y. *J. Appl. Polym. Sci.* **2012**, *125*, E334−E341.
(29) Gu, H.; Tadakamalla, S.; Zhang, X.; Huang, Y.; Jiang, Y.; Colorado, H. A.; Luo, Z.; Wei, S.; Guo, Z. *J. Mater. Chem. C* **2013**, *1*, 729−743.
(30) Moravkova, Z.; Trchova, M.; Tomsik, E.; Cechvala, J.; Stejskal, J. *Polym. Degrad. Stab.* **2012**, *97*, 1405−1414.
(31) Jin, C.; Nagaiah, T. C.; Xia, W.; Spliethoff, B.; Wang, S. S.; Bron, M.; Schuhmann, W.; Muhler, M. *Nanoscale* **2010**, *2*, 981−987.
(32) Li, L. M.; Liu, E. H.; Li, J.; Yang, Y. J.; Shen, H. J.; Huang, Z. Z.; Xiang, X. X.; Li, W. *J. Power Sources* **2010**, *195*, 1516−1521.
(33) Cochet, M.; Maser, W. K.; Benito, A. M.; Callejas, M. A.; Martinez, M. T.; Benoit, J.-M.; Schreiber, J.; Chauvet, O. *Chem. Commun.* **2001**, 1450−1451.
(34) Zengin, H.; Zhou, W.; Jin, J.; Czerw, R.; Smith, D. W., Jr.; Echegoyen, L.; Carroll, D. L.; Foulger, S. H.; Ballato. *Adv. Mater.* **2002**, *14*, 1480−1483.
(35) Feng, W.; Bai, X. D.; Lian, Y. Q.; Liang, J.; Wang, X. G.; Yoshino, K. *Carbon* **2003**, *41*, 1551−1557.
(36) J. Sainz, R.; Benito, A. M.; Martinez, M. T.; Galondo, J. F.; Sotres, J.; Baro, A. M.; Corraze, B.; Chauvet, O.; Maser, W. K. *Adv. Mater.* **2005**, *17*, 278−281.
(37) Ma, Y.; Cheung, W.; Wei, D.; Bogozi, A.; Chiu, P. L.; Wang, L.; Pontoriero, F.; Mendelsohn, R.; He, H. *ACS Nano* **2008**, *2*, 1197−1204.
(38) Kim, J.-W.; Lillehei, P. T.; Park, C. *J. Mater. Chem.* **2012**, *22*, 8408−8412.
(39) Cochet, M.; Louarm, G.; Quillard, S.; Buisson, J. P.; Lefrant, S. *J. Raman Spectrosc.* **2000**, *31*, 1041−1049.
(40) Tomsik, E.; Moravkova, Z.; Stejskal, J.; Trchova, M.; Salek, P.; Kovarova, J.; Zemek, J.; Cieslar, M.; Prokes, J. *Chem. Pap.* **2013**, *67*, 1054−1065.
(41) Zamora-Ledezma, C.; Blanc, C.; Maugey, M.; Zakri, C.; Poulin, P.; Anglaret, E. *Nano Lett.* **2008**, *8*, 4103−4107.
(42) Naraghi, M.; Filleter, T.; Moravsky, A.; Locascio, M.; Loutfy, R. O.; Espinosa, H. D. *ACS Nano* **2010**, *4*, 6463−6476.
(43) Li, Y.; Kröger, M. *Carbon* **2012**, *50*, 1793−1806.
(44) Hall, L. J.; Coluci, V. R.; Galvão, D. S.; Kozlov, M. E.; Zhang, M.; Dantas, S. O.; Baughman, R. H. *Science* **2008**, *320*, 504−507.